Modeling and Design of an Industrial Dryer with Convective and Radiant Heating

R. A. CAIRNCROSS,[1,*] S. JEYADEV,[2] R. F. DUNHAM,[2] K. EVANS,[2] L. F. FRANCIS,[1] and L. E. SCRIVEN[1,†]

[1]Department of Chemical Engineering and Materials Science and Center for Interfacial Engineering, University of Minnesota, Minneapolis, Minnesota 55455; [2]New Photoreceptor Product Development and Manufacturing, Xerox Corporation, Webster, New York 14580

SYNOPSIS

Industrial equipment for drying polymeric coatings normally consists of a series of zones, each with a controlled temperature and airflow. Drying of a polymer–solvent solution is strongly affected by the variation of diffusivity, solvent vapor pressure, and solvent activity with temperature and composition. The equations of mass transfer by diffusion and of heat transfer by conduction and radiation describe changes in composition and temperature within the shrinking coating. This system of equations is solved by Galerkin's method with finite element basis functions. The boundary conditions on dryer airflow and temperature change at the entrance to each zone. In a few test cases, the predictions show how evaporative cooling can slow drying in early zones where the coating temperature drops below the dryer temperature, whereas in later zones the coating temperature rapidly approaches the dryer temperature. Infrared heating can be used to reduce the extent of evaporative cooling. In the test cases and experiments, "blistering" occurs in later zones where high oven temperature causes the solvent partial pressure to rise; dryer parameters can be chosen to maintain solvent partial pressure just below ambient pressure in order to avoid "blistering" with least sacrifice of process speed.

INTRODUCTION

Coating of nonreactive polymeric solutions is necessarily followed by solvent removal, or drying. Poorly chosen drying conditions cause unwanted internal gradients, phase separations, inappropriate nonuniformities, and various stress-related failures or defects. An important goal is to understand, through experiment and theory, the mechanisms involved and their interactions well enough to be able to compute theoretical predictions that agree with measurements on laboratory and pilot plant drying processes, account for the performance of production processes, and permit optimization of the design and operation of equipment.[1]

In continuous liquid coating, beyond the take-away zone of the coater comes the drying zone, or zones. The conditions of airflow, solvent partial pressure, and temperature within each zone are chosen to achieve an acceptable residual solvent content at the end of the dryer. The residence time within the dryer is determined by the design production rate in a new installation or the maximum production rate of acceptable coating in an old one. Raising temperature and airflow enhances drying rate and can make higher process speed possible; however product quality may be degraded by bubble generation, or solvent boiling, and premature surface solidification, or "skinning." Frequently, the upper limit on process speed in a coating operation is determined by the dryer setup and the need to avoid defects caused by drying too fast or at too high of temperatures.[2] A sufficiently accurate theoretical model of the process enables the selection of operating conditions that yield a dried coating without these defects.

The rate of solvent removal from polymeric coatings is controlled by the diffusivity of solvents except when the polymer is dilute, the driving force for sol-

* Current Address: Sandia National Laboratories, Albuquerque, New Mexico 87185-0827.
† To whom correspondence should be addressed.

Journal of Applied Polymer Science, Vol. 58, 1279–1290 (1995)
 CCC 0021-8995/95/081279-12

vent removal in the gas is small, and the airflow is low. These diffusivities normally drop by many orders of magnitude as the solvents depart. Of course, the diffusivities rise at higher temperatures; so the dependence of diffusivity on both solvent concentration and temperature is a necessary part of any accurate theory of drying. Several researchers have measured diffusion coefficients and applied them to predicting drying of polymeric coatings.[3-5] The free volume theory of Vrentas and Duda has emerged as a convenient and accurate method for predicting diffusivities from limited experimental data in polymeric solutions above their glass transition temperature.[6,7] Theory of the formation of membranes by phase inversion also utilizes these diffusion theories. In phase inversion, solvent removal leads to unstable solutions that spinodally decompose to a bicontinuous structure, and after one continuous part is extracted, the porosity of the remaining network varies through the thickness of the membrane because of concentration gradients that develop during processing.[8,9]

The drying rate of a coating in an air impingement dryer is sometimes limited by low coating surface temperature due to evaporative cooling and frequently by low solvent diffusivity. To augment convective heat transfer, additional energy can be supplied directly to the bulk of the drying coating by exposing it to radiation that it can absorb. The resulting increase in coating temperature raises solvent diffusivity and volatility, and thus the drying rate. Radiant heating at infrared wavelengths can be a convenient way of accomplishing this, especially when the design of an existing dryer precludes using hotter air or stronger airflow.

In this paper, drying theory is used to model multiple-zone processes for drying polymer–solvent coatings. The theoretical model is derived from the one-dimensional mass and energy balances, standard constitutive relations, and appropriate boundary conditions. The theory predicts characteristic drying behavior in drying polymer coatings. This paper reports predictions of multiple-zone drying of a photoreceptor coating deposited as two layers of nonvolatile polymer in a single solvent, methylene chloride. The two layers differ chiefly in their absorbency of infrared radiation and are otherwise treated as one. The model is used to find the consequences of changing air temperatures and radiant energy delivery rates along an existing dryer. The outcome is insight into how to change design and operation of the dryer in order to eliminate blister defects.

DRYING THEORY

Drying of a coated liquid film in which the lateral variations in composition, temperature, and coating thickness are negligible is described by the transient one-dimensional convection–diffusion equations of heat and mass transfer, as shown for example by Cairncross et al.[10] In scaled form, the equations of mass and energy conservation are

$$\frac{du}{d\tau} = v_n \frac{\partial u}{\partial \xi} + \frac{\partial}{\partial \xi}\left(D \frac{\partial u}{\partial \xi}\right) \tag{1}$$

$$\frac{d\Theta}{d\tau} = v_n \frac{\partial \Theta}{\partial \xi} + \mathrm{Le} \frac{\partial}{\partial \xi}\left(\frac{\partial \Theta}{\partial \xi}\right) + Q_r \tag{2}$$

$u \equiv \rho_s/\rho_0$ is the concentration of methylene chloride in units of $\rho_0 = 1293\ \mathrm{kg/m^3}$, the initial solution density; $\xi \equiv z/h_0$ is the distance from the substrate in units of $h_0 = 1.72 \times 10^{-4}$ m; $D \equiv D(\rho_s, T)/D_0$ is the diffusion coefficient in units of $D_0 = 4.5 \times 10^{-9}$ $\mathrm{m^2/s}$, the initial diffusion coefficient; $\tau \equiv D_0 t/h_0^2$ is the time in units of $h_0^2/D_0 = 6.6$ s; $v_n \equiv \mathrm{v}_n h_0/D_0$ is the velocity of moving reference points in units of D_0/h_0; $\Theta \equiv (T - T_0)/(T_1 - T_0)$ is the temperature in units of $T_1 - T_0 = 10°\mathrm{C}$ where $T_0 = 16°\mathrm{C}$ is the initial coating temperature and $T_1 = 26°\mathrm{C}$ is an upper reference temperature; $\mathrm{Le} \equiv \kappa/(\rho_0 C_p D_0) = 672$ is the Lewis number, a measure of the mass to heat transfer resistances with $\kappa = 4.9\ \mathrm{W/m/°C}$ the thermal conductivity and $C_p = 1254\ \mathrm{J/kg/°C}$ the heat capacity; Q_r is the volumetric rate of heating by radiant energy absorption in units of $\rho_0 C_p (T_1 - T_0) D_0/h_0^2$. Initially the coating has uniform temperature and solvent concentration, $\Theta = 0$ and $u = 0.83$. The coating thickness is initially $h = 0.91$ in units of h_0.

Equation (1) expresses mass continuity when volume does not change on mixing and diffusion is described by Fick's law relative to a volume-averaged velocity (with the volume-averaged velocity equal to zero because there is no flux into the substrate). In the energy conservation eq. (2), the thermal diffusivity, $\kappa/\rho C_p$, is taken to be nearly independent of temperature and solution composition over the ranges of interest. The predictions of the theory show that because the Lewis number is large, temperature gradients are small, and hence the approximation of constant thermal diffusivity does not affect those predictions.

Solvent is removed from and energy is added to the coating by convective sweeping of its exposed surface by air of a specified temperature, airflow, and solvent partial pressure in each zone. Energy is

also added to the coating by convective sweeping of the backside of the web (substrate) by air of a specified temperature and airflow. The rates of transfer of mass and energy through the surface of the coating are described by transfer coefficients—lumped parameters that describe combined convective and diffusive or conductive transport processes occurring in the gas phase[10,11]:

$$-D\frac{\partial u}{\partial \xi} = 0, \quad \xi = 0 \tag{3}$$

$$-D\frac{\partial u}{\partial \xi} - uv_s = \mathrm{Bi}_m(\Pi^* a^s - \Pi^\infty), \quad \xi = h \tag{4}$$

$$\mathrm{Le}\frac{\partial \Theta}{\partial \xi} = \mathrm{Bi}_{hb}\mathrm{Le}(\Theta - \Theta^{b\infty}), \quad \xi = 0 \tag{5}$$

$$-\mathrm{Le}\frac{\partial \Theta}{\partial \xi} = \mathrm{Bi}_{hs}\mathrm{Le}(\Theta - \Theta^{s\infty}) + \mathrm{Bi}_m(\Pi^* a^s - \Pi^\infty)C_v, \quad \xi = h \tag{6}$$

Equation (3) expresses the lack of mass flux into the substrate. Equation (5) describes the heat transfer into the substrate. Equations (4) and (6) represent boundary conditions that are applied at the free surface of the coating where $\xi = h$. $\mathrm{Bi}_m \equiv k_m h_0 \rho_{g0}/D_0\rho_0$ is the coefficient of mass transfer from the surface of the coating, or mass Biot number; k_m is the mass transfer coefficient in units of length per time and is based on solvent concentration driving force in the gas phase, $\rho_{g0}(\Pi^* a^s - \Pi^\infty)$, where $\rho_{g0} = 0.71$ kg/m^3 is concentration of pure solvent vapor at T_1 and P_v^0, $\Pi^* \equiv P_v^*(T)/P_v^0$ is the vapor pressure of pure solvent at the surface of the coating in units of $P_v^0 = 0.57$ atm, Π^∞ is the concentration of solvent in the drying gas in units of ρ_{g0}, $a^s(\rho_s)$ is the solvent activity at the surface of the coating. $\mathrm{Bi}_{hb} \equiv k_{hb}h_0/\kappa$ is the coefficient of heat transfer through the substrate and backside airflow, or heat Biot number. The heat transfer coefficient $k_{hb} \equiv 1/(1/k_{h\mathrm{sub}} + 1/k_{h\mathrm{gasb}})$ accounts for heat conduction through the substrate ($k_{h\mathrm{sub}}$) and heat transfer through the gas on the back side of the substrate ($k_{h\mathrm{gasb}}$) in series. $\mathrm{Bi}_{hs} \equiv k_{hs}h_0/\kappa$ is the coefficient of heat transfer from the surface of the coating, or heat Biot number. Θ^∞ is the temperature of the bulk gas and $C_v \equiv \Delta H_v/C_p/(T_1 - T_0) = 23.3$ is the latent heat of vaporization of methylene chloride. In general, $k_{h\mathrm{gasb}}$ and k_{hs} differ, and so do $\Theta^{s\infty}$ and $\Theta^{b\infty}$, but in situations addressed in this paper it seemed reasonable to set them equal, and so they were. The solvent partial pressure in the bulk air, air temperatures, air velocities, and hence transfer coefficients change by steps from one zone to the next in the dryer and so the values in the model were changed at the entrance to each zone.

The velocity of the free surface is $v_s \equiv dh/d\tau$ in units of D_0/h_0 and is obtained from eq. (4) times the specific volume of the solvent in units of $1/\rho_0$, $\tilde{V}_s \equiv \hat{V}_s\rho_0 = 0.98$, (for methylene chloride), and the ideal mixing assumption:

$$v_s = -\tilde{V}_s\mathrm{Bi}_m(\Pi^* a^s - \Pi^\infty), \quad \xi = h \tag{7}$$

A field of reference points which move with the free surface but in proportion to their distances from the substrate surface, viz. with velocity $v_n = v_s\xi/h$ is employed in mapping of the drying coating onto a fixed domain in the solution of the equation system by Galerkin's method.

Drying characteristics predicted by this theory depend on the diffusivity, mass and heat transfer coefficients, solvent volatility, and latent heat of vaporization. Heat transfer coefficients of the impingement air jets in the dryer were predicted by the method of Gardon and Akfirat[12]; other correlations for various types of impingement nozzles types are available.[13] The mass transfer coefficients were estimated from the heat transfer coefficients by means of the Chilton–Colburn analogy.[11,14]

The partial pressure of the solvent is the product of the vapor pressure and the activity. The vapor pressure of pure solvent was obtained from the Antoine relation $\log(P_s^*) = a - b/(c + T)$; the parameters a, b, and c for methylene chloride are available in the literature.[15] The activity of the solvent in solution was predicted by the Flory–Huggins theory, $\ln(a^s) = \ln(1 - \Phi_p) + \Phi_p + \chi\Phi_p^2$, where Φ_p the volume fraction of polymer ($\Phi_p = 1 - u\tilde{V}_s$), and χ is the solvent–polymer interaction parameter which is 0.28 for the system in this paper.[16–18]

The sensitivity of drying to the diffusion coefficient hinges on its dependence on concentration and temperature as shown by Vrentas et al.[5] In polymeric solutions, diffusion coefficients generally drop as concentration of solvents fall, temperature declines, or molecular weight rises. Figure 1 shows the variation of the diffusion coefficient with solvent concentration and temperature for the methylene chloride/polymer solution studied in this paper. The diffusion coefficient in Figure 1 was calculated from the free volume theory of Vrentas and Duda,[6] which requires a set of free volume and diffusion parameters; the free volume parameters needed in this correlation were determined from the literature and intrinsic viscosity measurements. The remaining parameters (ξ_{VD}, ratio of molar volumes for solvent

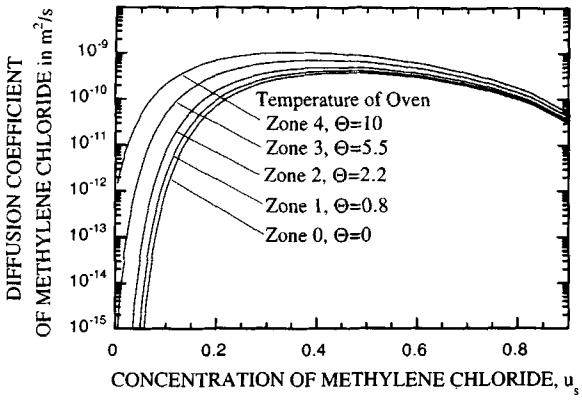

Figure 1 Diffusion coefficient in methylene chloride polymer solution varies with solvent concentration and temperature. Diffusion coefficient curves are shown at the oven temperatures. Estimated using Vrentas and Duda[6] free volume theory, free volume data from intrinsic viscosity measurements, and regression of drying model predictions to experimental data in Figure 2.

and polymer jumping units, and D_{10}, a constant preexponential factor) were chosen to obtain an acceptable fit between predictions of the one-dimensional convection diffusion equation and experimental measurement of residual solvents[19]; the quality of this fit was determined by inspection and the parameters ξ_{VD} and D_{10} were changed in a manual Picard iteration. This fit is shown by experimental data in Figure 2(a). At high temperatures the diffusivity drops by over three orders of magnitude, but at low temperatures, the diffusivity drops by many orders of magnitude. Thus the solution exhibits less diffusional resistance to drying at higher temperatures.

Radiant energy absorbed by the coating per unit volume per unit time adds a source term to the heat conduction equation. The infrared absorption was taken to be zero except in the fractional thickness β next to the substrate. The substrate has negligible absorptivity, and internal reflections were ignored. Beer's law describes the fall in radiation intensity through coating:

$$Q_r(\xi) \equiv I_0 \begin{cases} 0 & \beta h \le \xi \le h \\ \alpha \exp[-\alpha(\beta h - \xi)] & 0 \le \xi \le \beta h \end{cases} \quad (8)$$

I_0 is the intensity of the incident radiation, $\alpha = A/(\beta h_0)$ is the volumetric absorption coefficient with A the absorption coefficient. The incident volumetric heating strength, Q_r, the radiation flux, I_0, and the heat conduction rate are measured in units of $\rho_0 C_p(T_1 - T_0)D_0/h_0^2$. In the results in this paper $\alpha = 3$, and $\beta = 0.2$ and I_0 is specified in each dryer zone.

SOLUTION OF THE EQUATIONS

Equations (1) to (8) comprise a system of coupled nonlinear partial differential equations that are difficult if not impossible to solve in terms of standard analytical functions. They were solved by Galerkin's method with finite element basis functions.[20,21] The coefficients of the basis functions were found by solving a system of coupled differential-algebraic equations that express the requirement that the residual of each partial differential equation be orthogonal to the basis functions.[20] The coated layer was divided into ten finite elements with concentrations and temperature represented by each ele-

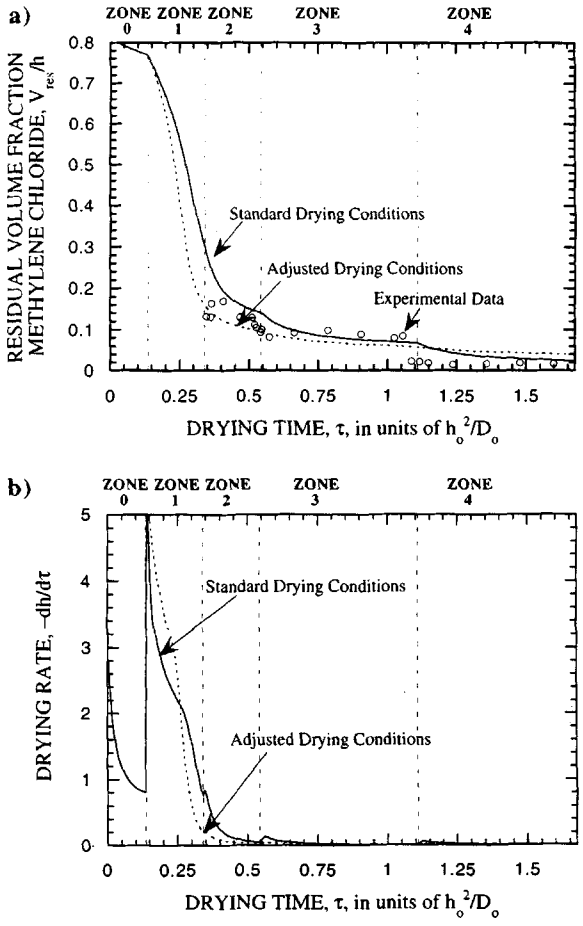

Figure 2 (a) Volume fraction of residual solvent (methylene chloride) in coating and (b) solvent evaporation rate with standard (solid line) and adjusted drying conditions (dashed line). Vertical lines mark the divisions between dryer zones. The data points mark measured solvent compositions from experiments.

Table I Typical Parameter Values of Methylene Chloride Polymer Solutions

$h_0 = 1.72 \times 10^{-4}$ m	Le = 672
$D_0 = 4.5 \times 10^{-9}$ m^2/s	$C_p = 1254$ J/kg/°C
$t_0 = h_0^2/D_0 = 6.6$ s	$C_v = 23.3$ (methylene chloride)
$\hat{V}_1 = 0.98$ (methylene chloride)	$T_0 = 16$°C
$\rho_0 = 1293$ kg/m^3	$T_1 = 26$°C
$P_v^0 = 0.57$ atm	$\rho_{g0} = 0.71$ kg/m^3 (methylene chloride)
$u_{i0} = 0.83$ $\Theta_0 = 0$	$h\ (\tau = 0) = 0.91$
$\chi = 0.28$	
Free Volume Parameters (as defined in 7)	
$D_{10} = 2.74 \times 10^{-8}$ m^2/s	E/R = 0°K
$V_1^* = 0.6247$ cm^3/g	$V_2^* = 0.733$ cm^3/g
$K_{11}/\gamma = 1.375 \times 10^{-3}$ cm^3/g/°K	$K_{21} - T_{g1} = -19$°K
$K_{12}/\gamma = 3.51 \times 10^{-4}$ cm^3/g/°K	$K_{22} - T_{g2} = -290$°K
$\xi_{VD} = 0.5$	

ment and quadratic basis functions. Thus, the domain is spanned by 21 basis functions, each associated with a node, and the values of temperature and methylene chloride concentration are defined as unknowns at each of these 21 nodes.

Because the concentration gradient is steepest in a diffusion boundary layer in concentration near the coating surface, the elements near the surface were made smaller than those near the substrate such that $\xi_j/h \equiv [(j-1)/(nn-1)]^2$ where ξ_j is the position of node j, and $nn = 21$ is the number of nodes. The nodes are not material points but move in proportion to the motion of the surface, $v_n \equiv v_s\xi/h$.

In the Galerkin formulation, the diffusion and conduction terms of the conservation equation's weighted residuals are integrated by parts with the divergence theorem, and the boundary conditions are applied to the resulting boundary terms. Three-point Gaussian integration evaluates the Galerkin residuals across each element.[20] The equation for the free surface velocity is an ordinary differential equation applied at the surface of the coating.

We used a nonlinear differential-algebraic equation system solver called DASSL[22,23] to solve this set of equations for the coefficients of the basis functions. DASSL uses a variable order backward differentiation formula in a predictor–corrector integration scheme. The nonlinear algebraic system at each time was solved by a quasi-Newton method, in which the matrix of sensitivities of the residual equations to the unknowns (Jacobian matrix) was recalculated only when Newton's method did not converge within a specified number of iterations. The matrix of sensitivities of the residual equations was a square matrix with 64 rows and columns. The matrix was mostly banded, but the free surface position unknown added a full column and full row to the matrix. Because the size of the matrix was relatively small, full matrix Gaussian elimination was used to solve the linear system. This linear system was solved and the vector of unknowns was updated until the root-mean-square norm of the residuals was less than 10^{-5} at each integration time-step. DASSL automatically chooses time integration step size and order of the backward differentiation formula to optimize speed of solution while maintaining the imposed error criteria. On a Cray Y-mp supercomputer, the computations in this paper took about 4.5 CPU seconds for the complete integration of about 600 unequally spaced time steps, or about 0.0075 CPU seconds per time step. On a Sun Sparcstation 10 with 64 MB of RAM, these results took about 16 CPU seconds for the complete integration of about 670 time steps, or about 0.024 CPU seconds per time step.

RESULTS

Convection Heating

The equation system was solved for air impingement drying of a coated layer of methylene chloride based photoreceptor in a five-zone dryer; the first zone, labeled Zone Zero, is the region of low airflow between the coating station and entrance to the air impingement dryer. The values of physical and reference parameters of this system are listed in Table I. The intensity of the incident radiant energy, I_0, and the solvent partial pressure in the drying air, Π^∞, are set to zero in the examples in this section. In principle and practice, the partial pressure of solvent in the drying air can be nonzero, but no advantage to raising the solvent partial pressure

emerged in a few cases explored, and it was always set to zero in the modeling. Oven temperatures and airflow rates, and hence the heat and mass transfer coefficients, were changed at the entrance to each zone. Table II shows the values of these parameters corresponding to two sets of drying conditions.

The standard set of parameters in Table II represents the drying conditions at which the experimental data shown in Figure 2(a) were previously collected, and the adjusted set represents the conditions which would maintain the highest possible air temperature zone-by-zone with no potential for solvent boiling. The oven temperatures in the adjusted parameter set were determined by manual Picard iteration to achieve a maximum solvent partial pressure within the coating between 0.99 and one atmosphere within each zone. Because methylene chloride concentration is highest near the base of the coating, the partial pressure is highest there, and the bubble point temperature is lowest there. Thus, the adjusted conditions were chosen so the coating temperature approached but did not exceed the bubble point temperature of methylene chloride at the base of the coating.

Figure 2(a) shows the predicted residual volume fraction of methylene chloride in the coating as a function of time (distance through dryer) for both sets of conditions given in Table II. The residual volume of methylene chloride per unit area of coating is calculated by integrating the volume fraction of methylene chloride, $u\bar{V}_s$, over the coating thickness $V_{res} \equiv \int_0^h u\bar{V}_s d\xi$, and the residual volume fraction is the residual volume divided by the coating thickness, V_{res}/h. Vertical lines in Figure 2(a) indicate transitions between zones; the transitions are sharp and instantaneous because step changes in the drying conditions were imposed between zones. The differences between the experimental data and theoretical data can be attributed to the experimental errors, intermixing of air between zones in the experiments, and uncertainty in some of the physical properties. Zone Zero shows little solvent removal; this zone has a low airflow because it corresponds to the takeaway zone between the coating head (where the liquid coating is deposited) and the entrance to the dryer. Most of the solvent escapes from the coating in Zone One where the solvent content is high and so diffusional limitations to drying are small. However, in Zone Two, the solvent residual volume fraction plateaus, indicating strong diffusional resistance to drying within the coating. In the last two zones, the solvent residual volume fraction does not change appreciably over the last 75% of each zone.

The rate of solvent evaporation, the drying rate, slows in later zones as shown in Figure 2(b) for both sets of drying conditions in Table II; the fall in drying rate is more pronounced than the plateaus in solvent residual volume fraction shown in Figure 2(a). In Figure 2(b), the evaporation rate peaks at the beginning of each zone then rapidly drops in a falling rate period indicative of diffusion controlled drying. The peak in the drying rate at the beginning of the zone corresponds to rapid solvent removal as the temperature of the coating and the diffusion coefficient rise. After the temperature levels, the drying process reaches a new falling rate period. In the last three zones, the drying rate drops to near zero, rendering most of the zone ineffective at solvent removal.

Figure 3 demonstrates the onset of diffusion-controlled drying at the standard drying conditions. This figure shows concentration profiles of methylene chloride through the coating at a series of times—each curve represents a single snapshot in time. The right end of each curve represents the position and concentration of the free surface of the coating (as time marches on and the coating shrinks, these curves end closer to the substrate and lower in solvent). The concentration of methylene chlo-

Table II Values of Dryer Parameters of Methylene Chloride Polymer Solution in Each Zone for Standard Drying Configuration and Adjusted Conditions Which Avoid Solvent Partial Pressures above 1 atm

	Standard Parameters					Adjusted Parameters				
	τ_{end}	Bi_m	$Bi_{hb}Le$	$Bi_{hs}Le$	Θ^∞	τ_{end}	Bi_m	$Bi_{hb}Le$	$Bi_{hs}Le$	Θ^∞
Zone 0	0.136	5	3	3	0	0.136	5	3	3	0
Zone 1	0.340	36	16.8	22.5	0.8	0.340	36	16.8	22.5	4.2
Zone 2	0.543	31.5	18.6	20.8	2.2	0.543	31.5	18.6	20.8	4.8
Zone 3	1.109	27.3	9.65	16.7	5.5	1.109	27.3	9.65	16.7	6.15
Zone 4	1.674	29.1	12.1	17.1	10	1.674	29.1	12.1	17.1	7.7

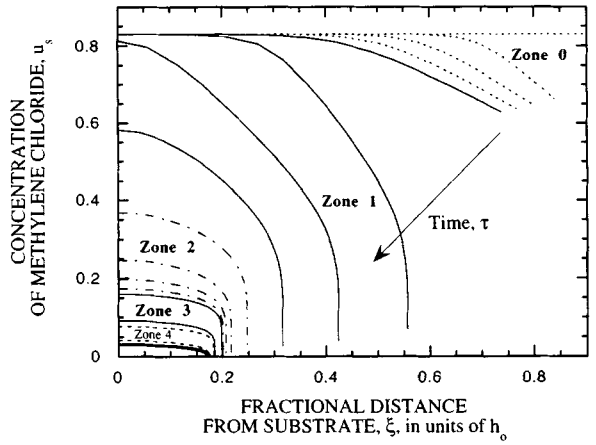

Figure 3 Profiles of methylene chloride concentration in a coating at a series of time intervals with standard drying conditions. Four concentration profiles are shown within each of the first three dryer zones (0, $\frac{1}{4}$, $\frac{1}{2}$, and $\frac{3}{4}$ of the way through the dryer), and two concentration profiles are shown within each of the last two zones (0 and $\frac{1}{2}$). The bold concentration profile indicates the concentration profile of solvent exiting the dryer.

ride is initially uniform, and in Zone Zero, the drying conditions are mild enough that only a small gradient in the methylene chloride concentration develops. However, in Zone One, the drying rate rises and diffusion of solvent to the surface cannot replenish the lost solvent fast enough; so the solvent concentration at the surface drops. Soon, the solvent concentration gradient steepens near the surface (in the middle of Zone One).

This region of steeply falling solvent concentration is indicative of diffusion controlled mass transfer and is often called skinning (or figurative skinning[24]). When the solvent concentration falls so low that the solidifying material can develop and support elastic stresses as it shrinks, skinning may cause defects through stress development or gradients in material properties. Also, it is commonly believed that skinning causes a fall in drying rates and a trapping of solvents that can be avoided by drying more slowly.[25] While the present theory, based on polymer solution behavior above the glass transition, does predict steep gradients in solvent concentration and diffusivity in Zones Two to Four, it does not—and apparently cannot—predict the type of skinning where more solvent can be removed in the same equipment under milder drying conditions anywhere within. In Zones One to Four, the Biot number, which represents the ratio of internal mass transfer resistance to external mass transfer resistance, is large: mass transfer is internally, or diffusionally, controlled. In each of the later zones, the sharp gradient in solvent concentration persists, but when the coating temperature rises, diffusion of solvents to the surface accelerates temporarily.

The temporary rise in solvent evaporation rate in the beginning of each zone arises from the rapid rise in temperature at the beginning of each zone as shown in Figure 4. Because the Lewis number, which is the ratio of heat transfer rate over mass transfer rate, is high, heat conduction through the coating is much faster than mass diffusion through the coating, and the temperature across the coating remains uniform. In these results, the temperature gradient across the coating was always less than $\Delta\Theta = 0.1$ or about 1°C. Also, in Zones Zero and One, the temperature of the coating drops below the oven temperature and the initial coating temperature. This drop arises from evaporative cooling when solvents evaporate so rapidly that heat supplied from the oven does not overcome the cooling. This phenomena does not occur in later zones because the drying is diffusion controlled and slow enough that the heat transfer rates can counteract evaporative cooling. Because B_{ih} is high in the last three zones, the coating temperature rises rapidly to the oven temperature then remains constant. This early transition period corresponds to the transition period for the solvent evaporation rate shown in Figure 2b. At the same time as the temperature rises to the zone temperature, the period of rapid solvent removal occurs.

Predicting Bubble Formation

Figure 5 shows the partial pressure of methylene chloride in the coating near the base and surface of

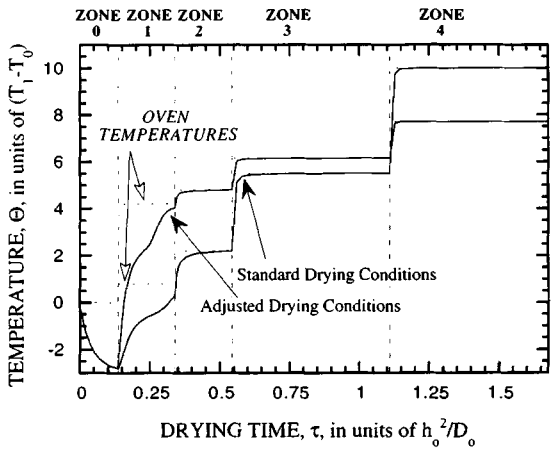

Figure 4 Temperatures of the coating and the oven within the coating with the standard and adjusted drying conditions. The higher partial pressure curve corresponds to solvent deep within the coating; this represents the maximum partial pressure. The lower corresponds to the solvent at the surface of the coating.

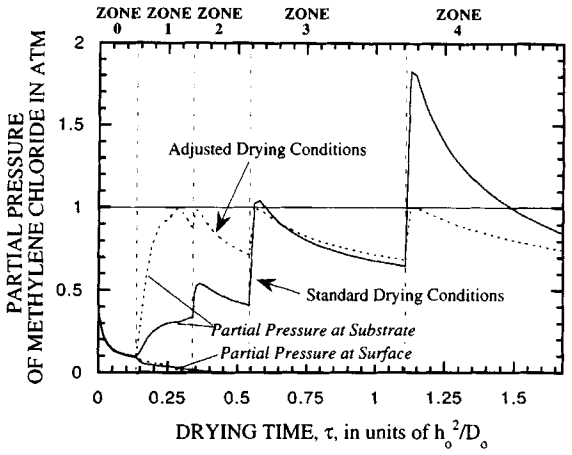

Figure 5 Partial pressure of methylene chloride within the coating with the standard and adjusted drying conditions. The higher partial pressure curve corresponds to solvent deep within the coating; this represents the maximum partial pressure. The lower corresponds to the solvent at the surface of the coating.

the coating with the standard and adjusted drying conditions. The solvent partial pressure, $\Pi(\Theta)\, a^s(u)$, is a function of both temperature and solvent concentration such that the partial pressure rises with increasing temperature or increasing solvent concentration. The two curves in Figure 5 represent the extremes in solvent partial pressure within the coating; the surface of the coating has the lowest partial pressure because the polymer concentration there is highest, while the base has the highest partial pressure because the polymer concentration there is lowest. The partial pressure of solvent at the surface of the coating rapidly drops to near zero due to diffusional resistance, further evidence for the drop in drying rate shown in Figure 2b. The partial pressure of solvent at the base of the coating, however, remains high. In the last two zones the partial pressure of solvent at the base rises above 1 atm, so boiling may occur in these zones. Experimentally, bubble formation was observed in the last two zones.

As shown in Figure 5, the partial pressure of solvent for the standard drying conditions rises far above 1 atm (almost to 2 atm) in Zone Four and slightly above 1 atm in Zone Three; whereas in the first three zones, the solvent partial pressure is far below 1 atm. Thus, the conditions in the coating are far from those that cause boiling in the first three zones, while the conditions in the coating are likely to cause boiling in the last two zones. The adjusted drying conditions reported in Table II were chosen to maximize the partial pressure of solvent in the coating without it exceeding 1 atm anywhere within the dryer; Figure 5 shows that this goal was met. The adjusted drying conditions differ from the standard conditions by higher temperatures in Zones One, Two, and Three but lower temperature in Zone Four. Since the oven temperature in Zone One for the adjusted conditions is much higher than for the standard conditions, much more solvent is removed in this zone under the adjusted conditions. The residual volume fraction of methylene chloride at the end of Zone One under adjusted conditions is about equal to the residual volume fraction of methylene chloride at the end of Zone Two under standard drying conditions; this means an equal amount of solvent was removed in one less zone by raising the temperature. However, to avoid partial pressures of methylene chloride above 1 atm, the temperature of Zone Four is lower under the adjusted conditions, and thus the final residual volume fraction of methylene chloride at the end of Zone Four ($\sim$ 4%) is about twice as high as under the standard conditions.

Evaporative cooling suppressed the drying rate significantly in the first two zones under standard conditions, but a higher oven temperature under the adjusted drying conditions brought about a rapid rise in the coating temperature in Zone One. This elevated temperature raised the diffusion coefficient and enabled more solvent to escape the coating without boiling the solvent. Thus, to obtain fastest solvent removal, the temperature of the oven should be as high as possible without producing defects or bubbles. In this paper, we are particularly interested in boiling and bubble formation, but avoidance of other defects could be equally well imposed as constraints in choosing drying conditions.

Subzoning: Splitting a Zone into a Series of Smaller Zones

The raised oven temperatures under the adjusted conditions help remove much more solvent in early zones, but Zones Three and Four still exhibit rapidly falling drying rates. Thus, as coatings become more concentrated in polymeric or nonvolatile material, the zones should become shorter, enabling a more gradual increase in the temperature of the coating. The benefits of subzoning, or splitting long zones into a series of smaller zones, are shown in Figures 6(a) and 6(b). In this example, Zones Three and Four were each split into 12 evenly spaced subzones and the oven temperature in the subzones increased by equal increments from $\Theta = 6.15$ for the first subzone in Zone Three and $\Theta = 10$ for the last subzone of Zone Four; in Zones Zero to Two, the adjusted drying conditions were used. Figure 6a shows the

coating temperature and bubble point temperature of the coating through the dryer. The coating temperature rises in a gradual, continuous manner for the subzoning conditions and does not rise above the bubble point temperature; bubble formation is not predicted for the subzoning conditions. The solvent content with the subzoning conditions is approximately the same as the standard conditions, as shown in Figure 6(b), but no bubbles form. Thus, subzoning results in better performance of an air convection dryer.

Of course, formation of bubbles is not determined solely by the partial pressure of solvents, it is also determined by nucleation and growth phenomena, or the number of bubble nucleation sites that exist within the coating and the rate at which bubbles grow once they are formed (which is determined primarily by the viscosity of the solution and the diffusion of solvent to the bubble surface). Likewise, bubbles may also be formed by mechanisms other than boiling, such as dissolution of dissolved gases.

Convection and Radiation Heating

The predictions computed from the drying model for a range of operating conditions accessible in the dryer show that bulk heating by infrared radiation is most beneficial in the early stages of the drying process. In these stages bulk heating greatly enhances the drying rate by reducing the evaporative cooling of the coating. Because the thermal diffusivity of the coating is high, the same effect can be achieved by increasing the air temperature in the upstream zones of the dryer (as in the case of the adjusted drying conditions discussed above). Whether adding infrared radiation or increasing air temperatures is a better solution will be determined by the economics of the individual processes.

The effect of incident radiation intensity on the solvent content in the coating is shown in Figure 7 using the standard drying conditions; the three curves in Figure 7(a) show results without infrared radiation, with equal infrared radiation through all the zones, and with infrared radiation intensities chosen to optimize drying without solvent partial pressures exceeding 1 atm (except in the last zone). Whereas the solvent content in the early zones is greatly reduced by the additional radiant heating, the final residual solvent content is lowered by only 1%. However, infrared radiation heating enables the length of the dryer to be reduced by one zone; the solvent content for the results with radiant heating is less than the solvent content with no radiant heating by enough that Zone Two could be eliminated from the radiant heating case and still result in the same residual solvent content as the no radiant heating case.

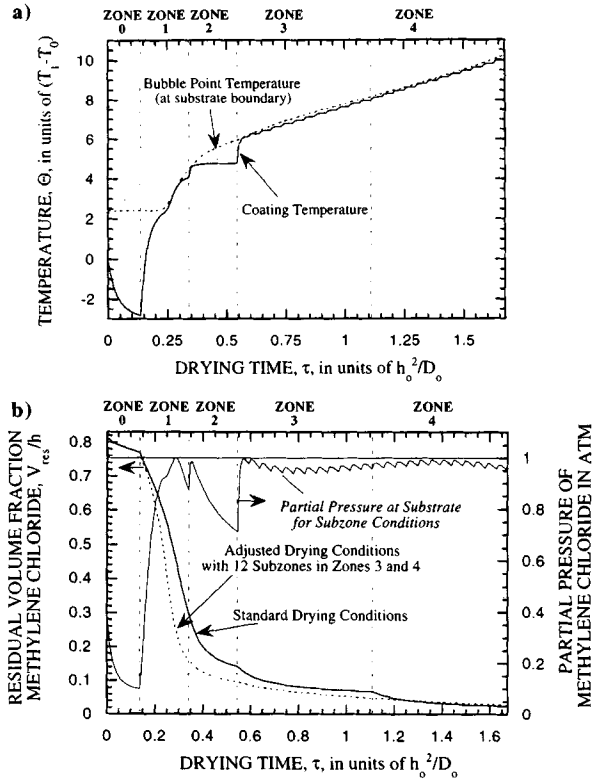

Figure 6 Predicted (a) coating temperatures and bubble point temperatures and (b) residual solvent levels for a dryer with subzones.

Radiant heating may also reduce the excess partial pressure of methylene chloride above atmospheric pressure, as shown in Figure 7(b); this could reduce the likelihood of bubble formation. The maximum solvent partial pressure within the coating is reduced from about 2 atm for no radiant heating to about 1.7 atm with the optimal radiant heating.

As solvent departs and its concentration drops, drying rate is increasingly restricted by the precipitously falling diffusivity. The fall can be countered somewhat by raising temperature, so long as bubble formation is avoided. Hence in the last two zones, the temperatures control the final level of the residual solvent. In those zones, infrared heating has no significant advantage over convective heating.

DISCUSSION

A useful theoretical model of drying a binary solvent–polymer solution has been constructed from standard heat and mass transfer correlations, vapor

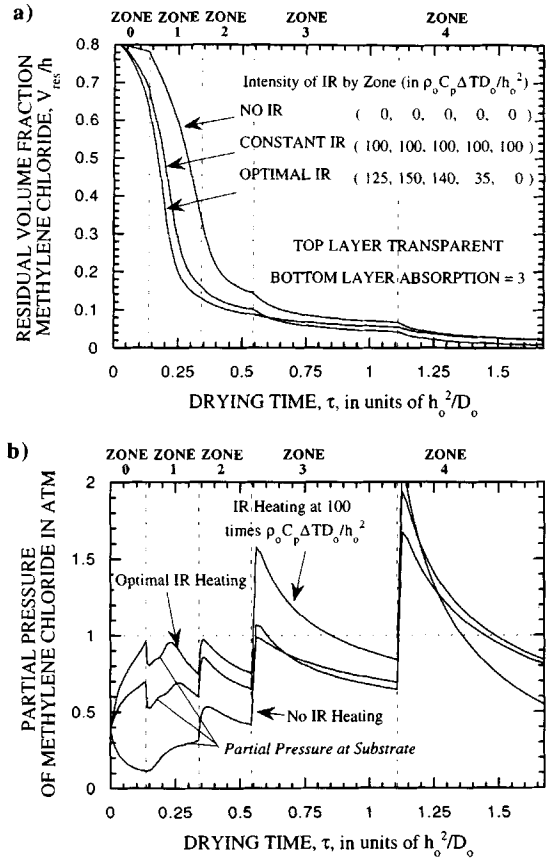

Figure 7 (a) Volume fraction of residual methylene chloride and (b) partial pressure of methylene chloride with several strategies of infrared heating. Vertical lines indicate boundaries between dryer zones.

liquid equilibrium relations, diffusion theory and correlations, and an approximation to Beer's law appropriate to infrared heating of thin coated layers. This theory has been used to help optimize the drying conditions in a multiple-zone dryer. We have demonstrated some general principles for dryer design: use as high a temperature as possible in early zones to overcome evaporative cooling and remove as much solvent as possible without creating defects (here defined as bubbles), and in later zones, use shorter zones (subzones) or zones with a gradual increase in temperature.

The model described in this paper establishes a framework on which to base dryer design and optimization of drying conditions. Optimization involves choosing an objective function (final residual solvent level, maximum temperature, or any other choice) and subjecting the objective to a set of constraints [operability limits of the heaters and fans, zone size, spacing of nozzles or IR lamps, limits in solvent partial pressure, temperature at which stable coating materials, solubility, or sharp concentration gradients (skinning), economic factors, or any other choice]. Unfortunately, no solution to the drying equations may exist within the limits set by the constraints, and the constraints may have to be relaxed. For example, solvent partial pressures in excess of 1 atm may be allowed in the last zone (as in the optimal IR example). Likewise, changing the size and number of zones may enable a better match with the objective function. For drying equipment that has already been built, the drying conditions can be found that most closely meet the objectives and the constraints, but the same method can be used to find a dryer design that best meets the demands of the process.

The model proves useful in establishing how infrared heating can be used to deliver heat to drying layers and thereby reduce the temperature difference between the oven and the cooler coating liquid. The payoff comes in quantitative predictions of how to control air temperature, air velocity, and incident infrared energy flux zone-by-zone in a multizone dryer, in order to achieve the lowest attainable residual solvent concentration without anywhere superheating the coating enough to generate deleterious vapor bubble within it. The effects of radiant heating can be achieved by convection drying at higher air temperatures, but radiant heating allows versatility of placing additional heating where it is needed. Radiant heating allows for greater flexibility in dryer design.

This work was supported by the National Science Foundation, through a Center for Interfacial Engineering fellowship for R. A. Cairncross, by industrial sponsors of the Coating Process Fundamentals Programs of the C.I.E., and by the State of Minnesota through the Minnesota Supercomputer Institute of the University of Minnesota and a Dissertation fellowship for R. A. Cairncross.

NOMENCLATURE

a^s	solvent activity at the surface of the coating
A	absorption coefficient
a, b, and c	Antoine coefficients
$\mathrm{Bi}_{hb} \equiv k_{hb}h_o/\kappa$	backside heat Biot number in units of h_0/κ
$\mathrm{Bi}_{hs} \equiv k_{hs}h_0/\kappa$	topside heat Biot number in units of h_0/κ

$\mathrm{Bi}_m \equiv k_m h_0 \rho_{g0}/D_0\rho_0$	mass Biot number
C_p	heat capacity (C_p = 1254 J/kg/°C)
$C_v \equiv \Delta H_v/C_p/(T_1 - T_0)$	latent heat of vaporization (C_{vs} = 23.3)
$D \equiv D(\rho_s, T)/D_0$	diffusion coefficient in units of D_0
D_0	initial diffusion coefficient ($D_0 = 4.5 \times 10^{-9}$ m^2/s)
D_{10}	preexponential factor in Vrentas–Duda free volume theory
h	thickness in units of h_0
h_0	reference thickness ($h_0 = 1.72 \times 10^{-4}$ m)
I_0	intensity of the incident radiation in units of $\rho_0 C_p(T_1 - T_0)D_0/h_0^2$
$k_{hb} \equiv 1/(1/k_{h\mathrm{sub}} + 1/k_{h\mathrm{gasb}})$	overall backside heat transfer coefficient
$k_{h\mathrm{gasb}}$, $k_{h\mathrm{gasb}}$	heat transfer through the gas on the back side of the substrate and topside of the coating
$k_{h\mathrm{sub}}$	heat transfer coefficient through substrate
k_m	mass transfer coefficient in units of length per time based on solvent concentration driving force in the gas phase, $\rho_{g0}(\Pi^* a^s - a^\infty)$
$\mathrm{Le} \equiv \kappa/(\rho_0 C_p D_0)$	Lewis number (Le = 672)
nn	number of nodes (nn = 21)
P_v^0	vapor pressure of pure solvent at T_1
P_s^*	vapor pressure of pure solvent from the Antoine relation
Q_r	radiant energy absorption in units of $\rho_0 C_p(T_1 - T_0)D_0/h_0^2$
T_0, T_1	initial coating and upper reference temperature (T_0 = 16°C and T_1 = 26°C)
$u \equiv \rho_s/\rho_0$	concentration of solvent in units of ρ_0
$v_n \equiv \mathrm{v}_n h_0/D_0 \equiv v_s\xi/h$	velocity of moving reference points in units of D_0/h_0
$v_s \equiv dh/d\tau$	velocity of free surface in units of D_0/h_0
$V_{\mathrm{res}} \equiv \int_0^h u_s \bar{V}_s d\xi$	residual volume per unit area of coating
$\bar{V}_s \equiv \hat{\mathrm{V}}_s\rho_0$	specific volume in units of $1/\rho_0$ ($\bar{V}_s$ = 0.98)
$\alpha \equiv A/(\beta h_0)$	volumetric absorption coefficient (α = 3)
β	fractional thickness of the absorbing layer next to the substrate (β = 0.2)
$\Theta \equiv (T - T_0)/(T_1 - T_0)$	temperature in units of $T_1 - T_0$
$\Theta^{b\infty}$, $\Theta^{s\infty}$	temperature of the bulk gas below and above coating
κ	thermal conductivity
$\xi \equiv z/h_0$	distance from the substrate in units of h_0
$\xi_j/h \equiv [(j-1)/(nn-1)]^2$	position of node j
ξ_{VD}	parameter from Vrentas–Duda free volume theory
Π^∞	solvent partial pressure in drying air in units of P_v^0 ($\Pi^\infty = 0$)
$\Pi^* \equiv P_v^*/P_v^0$	vapor pressure of pure solvent in units of P_v^0
ρ_{g0}	concentration of pure solvent vapor at T_0 and P_v^0
ρ_0	initial solution density (ρ_0 = 1293 kg/m^3)
ρ_s	solvent concentration
$\tau \equiv D_0 t/h_0^2$	time in units of h_0^2/D_0
τ_{end}	time at end of zone
Φ_p	volume fraction of polymer ($\Phi_p = 1 - u_s\bar{V}_s$)
χ	solvent–polymer interaction parameter from Flory–Huggins theory (χ = 0.28)

REFERENCES

1. R. A. Cairncross, L. E. Scriven, and colleagues, *Ind. Coatings Res.*, **4**, to appear.
2. E. D. Cohen and E. B. Gutoff, Eds. *Modern Coating and Drying Technology*, VCH Publishers, New York, 1992, Chap. 7.
3. M. Okazaki, K. Shoida, K. Masada, and R. Toei, *J. Chem. Eng. Jpn.*, **7**, 99 (1974).
4. Y. Sano, *Drying Technol.*, **10**, 591 (1992).
5. J. S. Vrentas, J. L. Duda, and H.-C. Ling, *J. Appl. Polym. Sci.*, **30**, 4499 (1985).
6. J. S. Vrentas and J. L. Duda, *J. Polym. Sci. Polym. Phys. Ed.*, **15**, 403 (1977).
7. J. M. Zielinski and J. L. Duda, *AIChE J.*, **38**, 405 (1992).
8. C. S. Tsay and A. J. McHugh, *J. Polym. Sci. Part B Polym. Phys.*, **28**, 1327 (1990).
9. J. E. Anderson and R. Ullman, *J. Appl. Phys.*, **44**, 4303 (1973).
10. R. A. Cairncross, L. F. Francis, and L. E. Scriven, *Drying Technol. J.*, **10**, 893 (1992).

11. E. J. Cussler, *Diffusion and Mass Transfer in Fluid Systems,* Cambridge University Press, New York, 1984.
12. R. Gardon and J. C. Akfirat, *J. Heat Transfer,* **88,** 101 (1966).
13. S. Polat, *Drying Technol.,* **11,** 1147 (1993).
14. T. H. Chilton and A. P. Colburn, *Ind. Eng. Chem.,* **26,** 1183 (1934).
15. R. M. Felder and R. W. Rousseau, *Elementary Principles of Chemical Processes,* John Wiley, New York, 1986.
16. P. J. Flory, *Principles of Polymer Chemistry,* Cornell University Press, Ithaca, NY, 1953.
17. H. Tompa, *Polymer Solutions,* Academic Press, New York, 1956.
18. J. Holten-Andersen and C. M. Hansen, *Prog. Org. Coatings,* **11,** 219 (1983).
19. P. E. Price, S. Wang, and I. H. Romdhane, *J. Polym. Sci. Part B Polym. Phys.,* to appear.
20. G. Strang and G. J. Fix, *An Analysis of the Finite Element Method,* Prentice-Hall, Englewood Cliffs, NJ, 1973.
21. B. A. Finlayson, *Numerical Methods for Problems with Moving Fronts,* Ravenna Park, Seattle, WA, 1992.
22. L. R. Petzold, *SIAM J. Sci. Statist. Comp.,* **3,** 367 (1982).
23. K. E. Brenan, S. L. Campbell, and L. R. Petzold, *Numerical Solution of Initial-Value Problems in Differential-Algebraic Equations,* Elsevier, New York, 1989.
24. R. A. Cairncross, Ph.D. thesis, University of Minnesota, 1994, available from University Microfilm International, Ann Arbor, MI.
25. G. W. Powers and J. R. Collier, *Polym. Eng. Sci.,* **30,** 118 (1990).

Received August 24, 1994
Accepted February 25, 1995